NRC Publications Archive
Archives des publications du CNRC

Strategic design of hemi-isoindigo polymer for a highly sensitive and selective all-printed flexible nitrogen dioxide chemiresistive sensor

Ngai, Jenner H. L.; Li, Zhao; Wang, Jia; He, Jinghui; Ding, Jianfu; Li, Yuning

This publication could be one of several versions: author’s original, accepted manuscript or the publisher’s version. / La version de cette publication peut être l’une des suivantes : la version prépublication de l’auteur, la version acceptée du manuscrit ou la version de l’éditeur.
For the publisher’s version, please access the DOI link below./ Pour consulter la version de l’éditeur, utilisez le lien DOI ci-dessous.

Publisher’s version / Version de l'éditeur:
https://doi.org/10.1002/smtd.202301521
Small Methods, 2024-02-06

NRC Publications Archive Record / Notice des Archives des publications du CNRC :
https://nrc-publications.canada.ca/eng/view/object/?id=98e72ce5-4b90-49ae-8819-c4c9157af76c
https://publications-cnrc.canada.ca/fra/voir/objet/?id=98e72ce5-4b90-49ae-8819-c4c9157af76c

Access and use of this website and the material on it are subject to the Terms and Conditions set forth at
https://nrc-publications.canada.ca/eng/copyright
READ THESE TERMS AND CONDITIONS CAREFULLY BEFORE USING THIS WEBSITE.

L’accès à ce site Web et l’utilisation de son contenu sont assujettis aux conditions présentées dans le site
https://publications-cnrc.canada.ca/fra/droits
LISEZ CES CONDITIONS ATTENTIVEMENT AVANT D’UTILISER CE SITE WEB.

Questions? Contact the NRC Publications Archive team at PublicationsArchive-ArchivesPublications@nrc-cnrc.gc.ca. If you wish to email the authors directly, please see the first page of the publication for their contact information.

Vous avez des questions? Nous pouvons vous aider. Pour communiquer directement avec un auteur, consultez la première page de la revue dans laquelle son article a été publié afin de trouver ses coordonnées. Si vous n’arrivez pas à les repérer, communiquez avec nous à PublicationsArchive-ArchivesPublications@nrc-cnrc.gc.ca.

National Research Council Canada
Conseil national de recherches Canada

Strategic Design of Hemi-Isoindigo Polymer for a Highly Sensitive and Selective All-Printed Flexible Nitrogen Dioxide Chemiresistive Sensor

*Jenner H. L. Ngai, Zhao Li, Jia Wang, Jinghui He, Jianfu Ding, and Yuning Li**

The study has developed two hemi-isoindigo (HID)-based polymers for printed flexible resistor-type nitrogen oxide (NO_2) sensors: poly[2-ethylhexyl 3-((3′“,4′-bis(dodecyloxy)-3,4-dimethoxy-[2,2′:5′,2′”-terthiophen]-5-yl)methylene)-2-oxoindoline-1-carboxylate] (P1) and poly[2-ethylhexyl 2-oxo-3-((3,3′“,4,4′-tetrakis(dodecyloxy)-[2,2′:5′,2′”-terthiophen]-5-yl)methylene)indoline-1-carboxylate] (P2). These polymers feature thermally removable carbamate side chains on the HID units, providing solubility and creating molecular cavities after thermal annealing. These cavities enhance NO_2 diffusion, and the liberated unsubstituted amide —C(=O)NH— groups readily form robust double hydrogen bonds (DHB), as demonstrated by computer simulations. Furthermore, both polymers possess elevated highest occupied molecular orbital (HOMO) energy levels of −4.74 and −4.77 eV, making them highly susceptible to p-doping by NO_2. Gas sensors fabricated from P1 and P2 films, anneal under optimized conditions to partially remove carbamate side chains, exhibit remarkable sensitivities of +1400% ppm^{-1} and +3844% ppm^{-1}, and low detection limit (LOD) values of 514 ppb and 38.9 ppb toward NO_2, respectively. These sensors also demonstrate excellent selectivity for NO_2 over other gases.

1. Introduction

Nitrogen dioxide (NO_2) is a prevalent air pollutant[1,2] known to cause health issues[3–5] and contribute to the formation of acid rain, which acidifies aquatic systems, disrupts natural ecology, pollutes soil, and damages infrastructures.[6–9] Additionally, NO_2 functions as a photochemical oxidant, facilitating the conversion of volatile organic compounds (VOCs) into secondary pollutants under sunlight. This process generates smog, leading to visual pollution, severe environmental damage, and respiratory issues in humans and animals.[10–12] The World Health Organization (WHO) recommends that humans and animals should not be exposed to NO_2 at a concentration exceeding 200 µg m^{-3} (0.53 ppm) for more than one hour.[13] Therefore, it is crucial to continuously detect and monitor the concentration of NO_2 in the environment. Moreover, NO_2 is generated as a by-product of nitro-containing explosives,[14] making it a potential indirect analyte for detecting the presence of such explosives.

Commonly used NO_2 gas sensors are chemiresistive devices using semiconducting metal oxides (MO_x) such as tin oxide (SnO_2) as sensing materials. Although MO_x-based NO_2 gas sensors offer high sensitivity and long-term stability, they suffer from poor selectivity and typically operate at high temperatures in the range of 200–600 °C,[15–17] which consumes significant energy and restricts device portability. In addition, the fabrication of MO_x-based sensors necessitates harsh conditions such as high vacuum, high temperature, and complex processing technology, resulting in increased sensor production costs.[18–21] These limitations impede the widespread adoption of MO_x-based NO_2 sensors.[22]

In recent years, the utilization of π-conjugated polymers as active sensing layers in gas sensors has garnered increasing attention.[23–30] This is due to their high sensitivity at or near room temperature, their structural adaptability for various target gases, and the cost-effective device fabrication achievable through printing techniques. Specifically, chemiresistive gas sensors employing π-conjugated polymers as active materials, known for their convenience in fabrication and operation, have demonstrated

---

J. H. L. Ngai, Y. Li
Department of Chemical Engineering and Waterloo Institute of Nanotechnology, (WIN)
University of Waterloo
200 University Ave West, Waterloo N2L 3G1, Canada
E-mail: Yuning.Li@uwaterloo.ca

J. H. L. Ngai, Z. Li, J. Ding
Security and Disruptive Technologies
National Research Council Canada
1200 Montreal Road, Ottawa, Ontario K1A 0R6, Canada

J. Wang, J. He
College of Chemistry
Chemical Engineering and Materials Science
Soochow University
Suzhou 215123, P. R. China

The ORCID identification number(s) for the author(s) of this article can be found under https://doi.org/10.1002/smtd.202301521

DOI: 10.1002/smtd.202301521

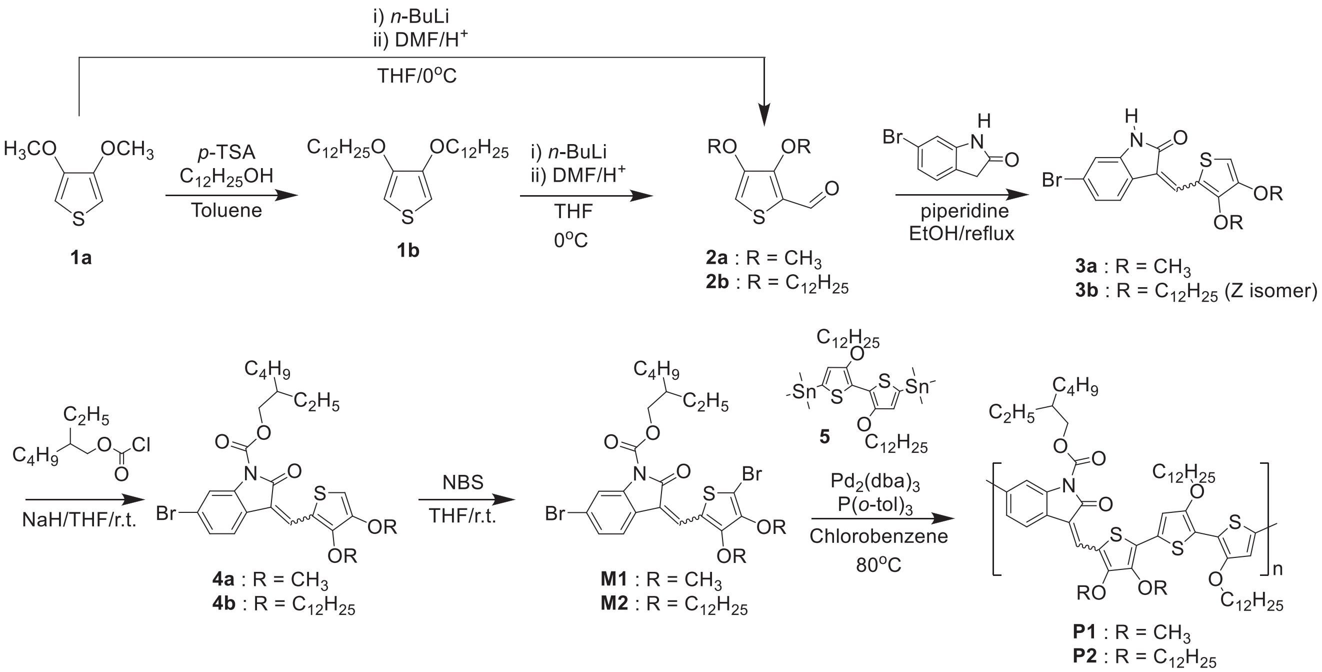

Scheme 1. Synthesis of polymers **P1** and **P2**.

remarkable sensitivity and selectivity toward NO_2.[31–33] When a π-conjugated polymer encounters an analyte, the response can encompass physical, chemical, or a combination of changes, such as alterations in morphology, chemical structure, redox reactions, and charge transfer. Charge transfer or doping represents an interaction between electron-rich (or p-type) conjugated polymers and oxidizing gases (like NO_2, SO_2, and PCl_3). This interaction increases the polymer's conductivity, leading to a surge in sensor output current.[34–37] Consequently, p-type conjugated polymer-based gas sensors exhibit greater sensitivity to oxidizing gases than non-oxidizing ones. To improve NO_2 sensitivity, the inclusion of polar side chains[38] and the utilization of conjugated building blocks capable of forming hydrogen bonds with NO_2 molecules[39] have shown to be effective strategies. Furthermore, the morphology of the sensing material plays a pivotal role in sensor sensitivity. To increase the surface area of the sensing material and enhance the diffusion of gas molecules, electrospun polymer nanofibers[40] and inorganic-organic hybrid polymer nanocomposites[41] have been employed. These materials have proven effective in detecting low-level gas analytes, achieving sensitivities down to parts per billion (ppb) concentrations. However, the fabrication processes for devices incorporating these materials involve complexities, including in-situ polymerizations, precise control of electrostatic self-assembly, and electrospinning. Most importantly, these materials suffer from inadequate printability, making it challenging to produce uniform thin films for consistently performing devices. Specialized techniques including phase inversion,[42,43] and breath-figure self-assembly method[33] have also been explored to introduce porosity and boost surface area. However, these methods are limited to creating relatively large micrometer-sized pores and are not well-suited for high-throughput, roll-to-roll printing processes.

In this study, we developed two p-type semiconductor polymers based on hemi-isoindigo (HID) that incorporate carbamate side chains for improved solubility and easy thermal removal after deposition. The thermal annealing process creates molecular cavities to facilitate the diffusion of NO_2 molecules. Furthermore, the liberated amide —C(=O)NH— groups on the HID units establish strong dual hydrogen bonds (DHB) with NO_2, as demonstrated by computer simulations, boosting sensitivity and selectivity. Additionally, strategically utilizing electron-rich alkoxy-substituted thiophene units raises the polymer's HOMO energy level, further enhancing NO_2 sensitivity. Our chemiresistive sensors utilizing these polymers demonstrate exceptional sensitivity, low LOD values, and superior selectivity for NO_2 over other gases. Notably, these sensors operate at room temperature with a driving voltage as low as 0.5 V.

2. Results and Discussion

2.1. Polymer Synthesis and Characterization

Polymers **P1** and **P2** were synthesized following the steps outlined in **Scheme 1**. Monomer **M1** was synthesized using 3,4-dimethoxythiophene (**1a**) as the starting material. The process involved formylation of **1a** through lithiation using *n*-butyllithium, followed by the addition of *N*,*N*-dimethylformamide at 0 °C to yield 3,4-dimethoxythiophene-2-carbaldehyde (**2a**). A piperidine-catalyzed Knoevenagel condensation reaction between **2a** and 6-bromooxinsole in refluxing ethanol produced 6-bromo-3-((3,4-dimethoxythiophen-2-yl)methylene)indolin-2-one (**3a**), existing as a mixture of (*Z*) and (*E*) geometric isomers at a 1:1 ratio. Without separating the isomers, **3a** underwent a carbamation reaction to yield 2-ethylhexyl 6-bromo-3-((3,4-dimethoxythiophen-2-yl)methylene)−2-oxoindoline-1-carboxylate (**4a**). Subsequent

Table 1. Optical, electrochemical, and physical properties of **P1** and **P2**.

Polymer	λ_{max} [nm]		λ_{onset} [nm]		HOMO$_{CV}$ [eV]	LUMO$_{opt/CV}$ [eV]	E$_{g,opt}$ [eV]	M$_w$	M$_n$	Đ
	sol.	Film	sol.	film	film	film	film	–	–	–
P1[a]	688	694	867	919	−4.74	−3.39	1.35	12398	7635	1.62
P2	680	721	821	1004	−4.77	−3.54	1.23	17964	10204	1.76

[a] The optical, electrochemical properties, and molecular weights of **P1** had been reported in a previous literature by the same principal authors.[44]

bromination using *N*-bromosuccinimide (NBS) resulted in 2-ethylhexyl 6-bromo-3-((5-bromo-3,4-dimethoxythiophen-2-yl)methylene)−2-oxoindoline-1-carboxylate (**M1**), present as a mixture of (*Z*) and (*E*) isomers in a 1:1 ratio.

Monomer 2-ethylhexyl (*Z*)−6-bromo-3-((5-bromo-3,4-bis(dodecyloxy)thiophen-2-yl)methylene)−2-oxoindoline-1-carboxylate (**M2**) was synthesized similarly to **M1**. The process involved the transetherification of **1a** with 1-dodecanol to obtain 3,4-bis(dodecyloxy)thiophene (**1b**). Formylation of **1b** was carried out using *n*-butyllithium and dimethylformamide at 0°C, resulting in 3,4-bis(dodecyloxy)thiophene-2-carbaldehyde (**2b**). A piperidine-catalyzed Knoevenagel condensation reaction between **2b** and 6-bromooxinsole yielded the pure geometric isomer (*Z*)−3-((3,4-bis(dodecyloxy)thiophen-2-yl)methylene)−6-bromoindolin-2-one (**3b**). Carbamation of **3b** led to 2-ethylhexyl 3-((3,4-bis(dodecyloxy)thiophen-2-yl)methylene)−6-bromo-2-oxoindoline-1-carboxylate (**4b**) as a mixture of (*Z*) and (*E*) isomers (Z:$E \approx$ 1:1). Bromination of **4b** using NBS produced 2-ethylhexyl 6-bromo-3-((5-bromo-3,4-bis(dodecyloxy)thiophen-2-yl)methylene)−2-oxoindoline-1-carboxylate (**M2**) as a mixture of (*Z*) and (*E*) isomers (Z:$E \approx$ 7:1).

Stille polymerization was subsequently carried out using (3,3′-bis(dodecyloxy)-[2,2′-bithiophene]−5,5′-diyl)bis(trimethylstannane) (**5**) and either **M1** or **M2** to yield **P1** and **P2**, respectively. The molecular weights of these polymers were characterized using high-temperature gel-permeation chromatography (HT-GPC), with results provided in **Table** 1 and Figure S1 (Supporting Information).

Thermogravimetric analysis (TGA) was employed to investigate the thermal stability of the polymers. The TGA plots revealed that, when heated at 250 °C in air for 20 min, ≈78% of the carbamate side chains in **P1** and 59% in **P2** were removed (Figure S3, Supporting Information). This removal process resulted in the release of unsubstituted amide —C(═O)NH— groups on the HID units.[44,45] To further characterize the polymers, attenuated total reflectance infrared (ATR-IR) spectroscopy measurements were conducted on **P1** and **P2** after annealing at 250 °C. As shown in **Figure** 1a,b, prior to thermal annealing, both **P1** and **P2** exhibited characteristic carbamate side chain functional vibrations, including the C-N bending (ν_a = 1096, and ν_a’ = 1097 cm^{-1}), C-O bending (ν_b = 1153, and ν_b’ = 1153 cm^{-1}), C–N stretching (ν_c = 1537, and ν_c’ = 1417 cm^{-1}), and C═O stretching (ν_d = 1775, and ν_d’ = 1774 cm^{-1}) (Figure 1). After thermal annealing, these characteristic peaks weakened or even disappeared. Concurrently, a broad band in the range of 3200–3600 cm^{-1} emerged for both polymers, originating from the characteristic N–H stretching of the liberated –C(= O)NH– groups. Within this broad peak, a small peak at ν_e = 3444 cm^{-1} was observed, which could be attributed to the stretching frequency of the free (non-bonded) amide N-H groups,[46–49] while other peaks around 3400 cm^{-1} corresponded to the stretching of hydrogen-bonded amide N-H groups.[49–51] These IR results confirm the facile thermal removal of carbamate groups, resulting in the liberation of —C(═O)NH— groups.

2.2. Optical and Electrochemical Properties

Ultraviolet–visible-Near-Infrared (UV–vis-NIR) spectroscopy was used to study the light absorption properties of the polymers. In chloroform solutions, **P1** and **P2** exhibited significantly red-shifted absorption peaks at (λ_{max} = 688 and 680 nm, respectively)

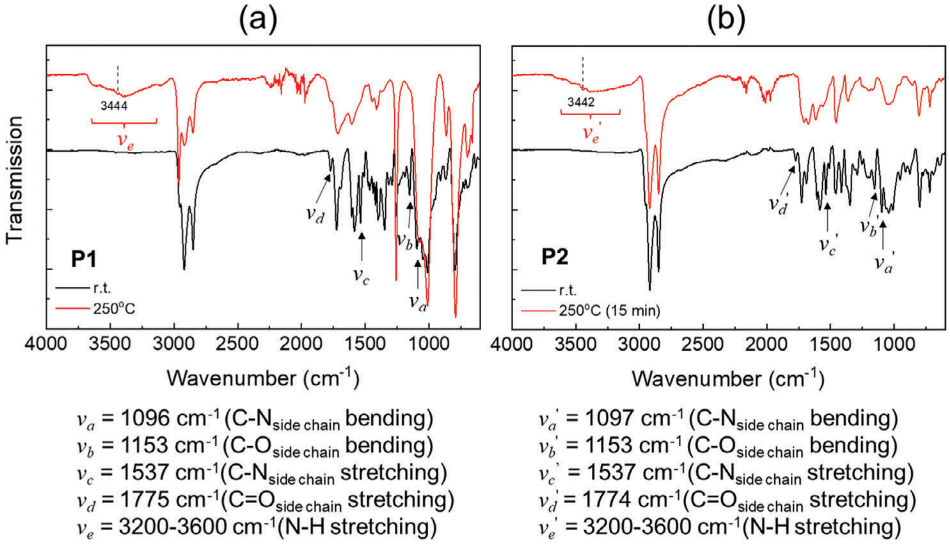

Figure 1. ATR-IR spectra of a) **P1**; and b) **P2** before and after thermal annealing at 250 °C for 15 min in ambient air.

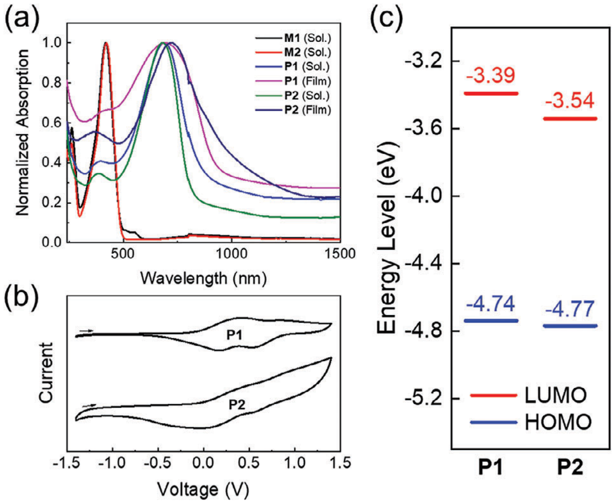

Figure 2. a) UV–vis-NIR spectra of monomers **M1** & **M2** and polymers **P1** & **P2** in chloroform solutions and as-cast films dried at room temperature. b) Cyclic voltammograms (versus Ag/AgCl) of **P1** and **P2**. c) Energy levels of **P1** and **P2** determined from CV diagrams and UV–vis spectra.

in comparison to their monomers **M1** and **M2** (λ_{max} = 420 nm) (**Figure** 2a and Table 1). This redshift in the absorption spectra of the polymers suggests an extension of their π-conjugation length relative to the monomers. Moreover, when examining the UV-Vis-NIR spectra of the as-cast **P1** and **P2** films, we observed additional red shifts of 6 and 41 nm, respectively, in λ_{max} compared to their solutions (Figure 2a). These shifts indicate the formation of *J*-aggregates resulting from interchain π-π interactions in the solid state. Notably, the more substantial red shift in **P2**, transitioning from solution to the solid state in comparison to **P1**, can likely be attributed to the longer dodecyloxy side chains, which may facilitate the self-assembly of polymer chains into a more planar backbone conformation.[52] This better chain packing and increased crystallinity in **P2** were confirmed by XRD data, as discussed later.

The incorporation of the electron-rich 3,3′-bis(dodecyloxy)−2,2′-bithiophene unit into the polymer backbone was intended to raise the HOMO energy level of the polymer, facilitating electron transfer from the polymer to the electron-deficient NO_2.[53] Cyclic voltammetry (CV) measurements of the polymer films were carried to determine the HOMO energy levels of **P1** and **P2.** Both polymers exhibited distinctive oxidation processes, with no observed reduction processes due to their highly electron-rich nature (Figure 2b). The calculated HOMO energy levels for **P1** and **P2** were −4.74 and −4.77 eV, respectively, using ferrocene as the standard, which has a HOMO energy of −4.8 eV.[54] The LUMO energy levels were subsequently calculated from their HOMO energy levels and optical band gaps, determined from the UV-Vis-NIR absorption onsets, to be −3.39 eV for **P1** and −3.54 eV for **P2** (Figure 2c and Table 1).

2.3. Fabrication and Testing of Chemiresistive Gas Sensors

The fabrication of chemiresistive sensors involved drop-casting a 5 µL solution (0.625 mg mL^{-1} in chloroform) of **P1** or **P2** onto the top insulating SiO_2 layer of a SiO_2/Si wafer substrate, resulting in a 30 nm thick polymer thin film. The substrate featured gold interdigitated electrode pairs with a channel length of 5 µm and a channel width of 2 mm (with a W/L ratio of 400). The sensors underwent annealing at various temperatures, ranging from room temperature to 250°C, and were subsequently tested using a custom-built gas sensing system (Figure S2, Supporting Information).

The gas sensing test was conducted by applying a DC voltage to the two interdigitated electrodes of the sensor while utilizing dry N_2 or air as the carrier gas at a total flow rate of 300 mL min^{-1}. Gases with various NO_2 concentrations were prepared by blending NO_2 with carrier gases in different ratios, all while maintaining a constant total flow rate. The temperature of the gas sensor chamber was maintained at 25.0°C with the assistance of an Omega CN32PT-330 temperature controller. Sensor current was recorded as a function of time (*I*–*t*) or voltage (*I*–*V*) employing a Keysight B2902A Precision Source/Measure Unit. During dynamic sensing tests, at each NO_2 concentration level, the gas was introduced for 50 s, followed by a 250 s recovery period under continuous carrier gas flow before commencing the next cycle. The *I*–*V* characteristics of the NO_2 sensors were measured under a gas flow at constant NO_2 concentrations, ranging from 167 ppb to 4.00 ppm, with the devices scanned from 0 to 1.0 V.

Figure 3 illustrates the dynamic sensing responses (*I*–*t*) of the sensors with polymer films annealed at 150 °C when exposed to increasing concentrations of NO_2 gas. In the absence of NO_2 gas, the baseline currents for sensors based on **P1** and **P2** were 1.67 and 0.011 nA, respectively. Following exposure to NO_2 gas, both sensors exhibited increased currents. This interaction between the polymers and NO_2 is attributed to a charge transfer process, wherein electrons from the electron-rich polymer backbone were drawn by the electron-deficient oxidant NO_2, leading to the generation of delocalized holes or polarons as the primary charge carriers in the polymer.[20,31,55–57] Given that the reduction potential of NO_2 is 0.80 V versus normal hydrogen electrode (NHE),[58] NO_2 possesses an electron affinity (EA) of 5.24 eV or a LUMO energy of −5.24 eV, based on the energy levels relative to the standard hydrogen electrode (SHE), which is −4.44 eV relative to the vacuum (0 eV).[59] Clearly, electron transfer from the high-lying HOMO energy levels of **P1** (−4.74 eV) and **P2** (−4.77 eV) to the LUMO of NO_2 is energetically favorable. This electron transfer from **P1** or **P2** to NO_2 (or p-doping) resulted in increased polymer conductivity and elevated device current.

The dynamic sensing responses of polymers annealed at other temperatures are provided in Figures S4 and S5 (Supporting Information). Unexpectedly, devices annealed at high temperatures above 200 °C exhibited no response. This is surprising considering our prior study,[44] which demonstrated that **P1** annealed at an even higher temperature of 250 °C could be doped by F4TCNQ that has a weaker electron affinity (E_{LUMO} = −5.01 eV) than NO_2 (E_{LUMO} = −5.24 eV).[58,59] This phenomenon is likely caused by the excessive removal of carbamate side chains, deactivating the —C(=O)NH— groups due to the formation of interchain hydrogen bonds, as further discussed in subsequent sections.

The *I*–*V* characteristics of sensors annealed at the optimized temperature (150 °C) and exposed to NO_2 gases with varying concentrations ranging from 167 ppb to 4 ppm are presented in Figure 3c,d. Prior to NO_2 gas exposure, the *I*-*V* curves of

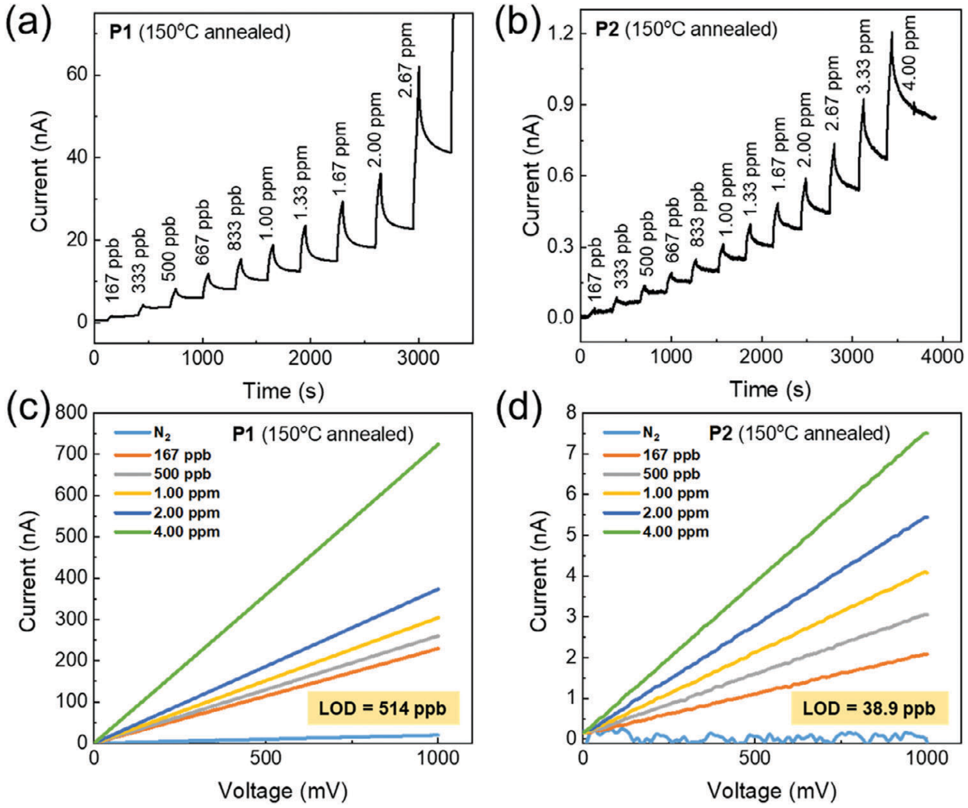

Figure 3. a) Dynamic sensing response of sensors by applying a D/C bias voltage of 500 mV upon exposure to NO_2 gas for Polymer **P1** from 167 ppb to 2.67 ppm (refer to Figure S4d, Supporting Information for sensing data at 4.00 ppm NO_2); and b) **P2** from 167 ppb to 4.00 ppm; c,d) *I*–*V* characteristics of NO_2 sensors exposed to a gas flow at constant NO_2 concentrations ranging from 167 ppb to 4.00 ppm. The devices were scanned from 0–1.0 V. All devices were annealed at 150 °C.

the device based on the **P1** film displayed Ohm's Law behavior, indicated by a linear *I*–*V* relationship passing through the origin. This observation indicates that, even in the absence of NO_2, the **P1** film displayed a notable conductivity of 1.66×10^{-5} S cm^{-1}. This ohmic *I*–*V* relationship can be attributed to the p-doping of the electron-rich **P1** by oxygen in the ambient air, a phenomenon commonly observed in highly electron-rich p-type polymers, such as poly(3-hexylthiophene).[60–64] In contrast, the device based on **P2** only exhibit noise signals before exposure to NO_2. Upon exposure to NO_2, both polymers displayed an increase in current with rising NO_2 concentration, characterized by steeper slopes in their *I*–*V* curves (Figure 2). This behavior is indicative of increased NO_2 doping, a characteristic of chemiresistive-type sensors. Utilizing the *I-V* relationship presented in Figure 3c,d as calibration curves, the limit of detection (LOD) for the optimized **P1** and **P2** devices was determined to be 514 and 38.9 ppb, respectively, in accordance with the IUPAC's recommendation.[65–67] Remarkably, the LOD values for both polymers, especially for the **P2**-based device, are on par with those of other highly sensitive NO_2 sensors based on small molecules and inorganic materials.[31,68–70]

Overall, the **P2**-based device exhibited an absolute current approximately two orders of magnitude lower than that of the **P1**-based device at the same NO_2 concentration, indicating its lower conductivity. Specifically, when exposed to 4 ppm NO_2, the calculated conductivity of the polymer channel was 6.04×10^{-4} S cm^{-1} for **P1** and 6.25×10^{-6} S cm^{-1} for **P2**. **P2** features longer dodecyloxy groups on the bithiophene comonomer units, resulting in increased interchain distances compared to **P1**, which has shorter methoxy groups. This longer interchain distance in **P2** hinders charge transport, contributing to its lower conductivity. Additionally, **P2** possesses a slightly lower HOMO energy level (−4.77 eV) compared to **P1** (−4.74 eV), making the charge transfer from **P2** to the dopant NO_2 (or O_2) more challenging.

2.4. Sensor Sensitivity and Device Optimization

The sensitivity of a sensor to a particular analyte can be quantified using Equation (1):[71,72]

$$\text{Sensitivity} = \frac{\Delta I / I_{\text{inert}}}{C} \times 100\% \tag{1}$$

where I_{inert} represents the initial current measured in an inert environment, such as under N_2, prior to exposure to the analyte gas, and ΔI is the change in current, defined as $I - I_0$, where I_0 and I are the baseline current before introducing an analyte at a concentration C and the maximum current (I) recorded after introducing the analyte. $\Delta I / I_{\text{inert}}$ is commonly referred to as the response of the device at a specific analyte concentration.[72]

It is noteworthy that in a dynamic sensing test involving multiple analyte gas feeds, characterized by a drifting baseline (poor

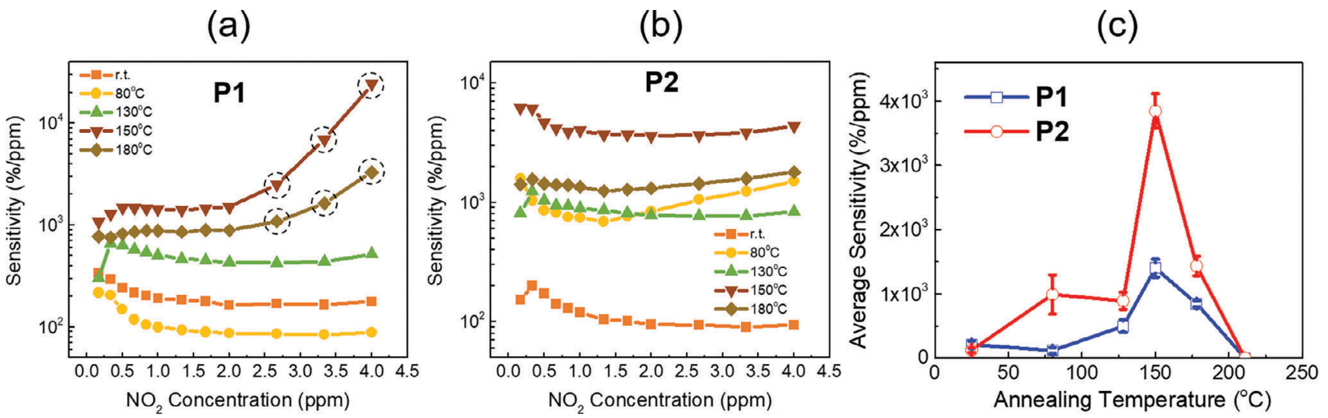

Figure 4. a,b) Sensitivities of sensor devices based on **P1** and **P2** films annealed at different temperatures and at different NO_2 concentrations. Circled data points in (a) may have been overestimated because the devices showed poor recovery (Figure S4, Supporting Information). c) The average sensor sensitivities of devices measured in the NO_2 concentration range between 167 ppb and 4.00 ppm with sensors annealed at different temperatures. Each error bar represents the sensitivity variation across a NO_2 concentration range shown in (a) and (b) (with some data points marked with dashed circles excluded) at a specific annealing temperature for the same device. The devices were annealed for 15 min at each annealing temperature. The devices were operated at 500 mV.

baseline recovery), as depicted in Figure 3a,b, I_0 is identical to I_{inert} for the initial feed but undergoes changes after the initial analyte exposure. Consequently, it is crucial to use the baseline current of a fresh device or a fully recovered device to establish I_{inert}, ensuring consistent sensitivity values. In practical applications, a pair of sensors is often employed, consisting of an encapsulated reference sensor for background correction (obtaining a relatively constant I_{inert} unaffected by the sensing environment) and a working sensor for analyte detection (yielding ΔI). These two sensors operate simultaneously, ensuring precise and accurate measurements.

Figure 4a,b depict the sensitivities of devices based on **P1** and **P2** films annealed at various temperatures, calculated using Equation (1) based on dynamic sensing responses recorded at different NO_2 concentrations (Figures S4 and S5, Supporting Information). Devices employing **P1** films annealed at temperatures below 130 °C exhibited rapid response and excellent recovery within the measured NO_2 concentration range from 167 ppb to 4 ppm (Figure S4, Supporting Information) and maintained relatively stable sensitivity in the NO_2 concentration range of 1 to 4 ppm (Figure 4a). However, at higher annealing temperatures of 150 and 180 °C, the **P1** devices exhibited poor recovery at NO_2 concentrations above 2 ppm, suggesting substantial trapping of NO_2 gas within the **P1** film. This resulted in abnormally high sensitivities at these elevated NO_2 concentrations. In contrast, all **P2** devices demonstrated swift response with effective recovery and consistent sensitivity across the tested NO_2 concentration range (Figure S5, Supporting Information; Figure 4a).

The sensitivity of both **P1** and **P2** devices showed significant dependence on the annealing temperature, as illustrated more clearly in Figure 4c, which presents plots of the average sensitivity obtained at different concentrations versus the annealing temperature. For the reasons mentioned earlier, data points measured at NO_2 concentrations above 2.67 ppm were excluded from the calculation of the average sensitivity for **P1**-based sensors annealed at 150 °C and 180 °C. Without annealing (room temperature), **P1** and **P2** devices exhibited average sensitivities of +210 and +125%ppm^{-1}, respectively. When the polymer films were annealed at 80 °C, the **P1**-based device displayed a reduced sensitivity of +118%ppm^{-1} compared to the non-annealed device, while the **P2**-based device exhibited a substantial increase in sensitivity to +990%ppm^{-1}. At a higher annealing temperature of 130 °C, the sensitivity of the **P2**-based device changed only slightly (+890%ppm^{-1}), while the sensitivity of the **P1**-based device increased to +497%ppm^{-1}. At an annealing temperature of 150 °C, both **P1** and **P2**-based devices exhibited a remarkable increase in sensitivity, reaching +1400 and +3844%ppm^{-1}, respectively. Annealing at 180 °C resulted in reduced sensitivity for both **P1** and **P2** devices, to +1138 and +1434%ppm^{-1}, respectively. Further elevating the annealing temperature to 210 °C led to a complete loss of sensitivity in both sensors. The above results indicate that the highest sensitivity for both **P1** and **P2** sensors was achieved at an annealing temperature of 150 °C.

2.5. Sensor Selectivity Study

To assess the selectivity of **P1** and **P2**-based sensors, we conducted tests with six other common gases: sulfur dioxide (SO_2), ammonia (NH_3), formaldehyde (CH_2O), ethylene (C_2H_2), hydrogen sulfide (H_2S), and hydrogen (H_2). Initially, we used nitrogen (N_2) as an inert carrier gas. Sensitivity to these analyte gases was measured and calculated, following the same procedure as for NO_2, and compared to the sensitivity to NO_2 at the same concentration to determine sensor selectivity.

Remarkably, both the **P1** and **P2** sensors exhibited very low sensitivity to all four interfering gases, even at a high analyte concentration of 4 ppm. Given the concentration-dependent nature of sensor sensitivity, it was essential to maintain consistent concentrations of interfering gases and NO_2 for a fair comparison. A **P1** device annealed at 130 °C and a **P2** device annealed at 150 °C were selected for this study, as these devices demonstrated the highest sensitivity and effective signal recovery at a NO_2 concentration of 4 ppm. Specifically, **P1** and **P2**-based sensors were subjected to four sensing cycles for each gas. Each cycle introduced an analyte at a concentration of 4 ppm for 50 s, followed by a

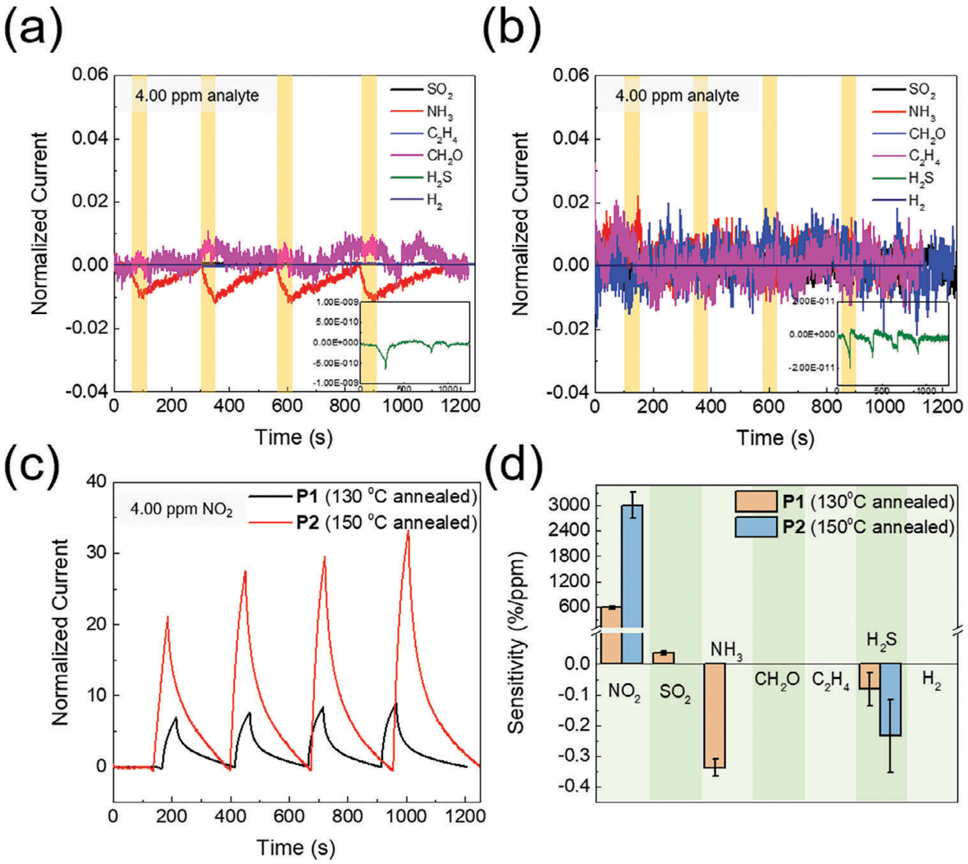

Figure 5. Dynamic sensing response of a) 130 °C annealed **P1**-based and b) 150 °C annealed **P2**-based sensors toward six different gases at a concentration of 4.00 ppm injected at different time intervals. Orange shaded areas show the approximate time when the analyte was being introduced. The subset graphs show magnified views of the responses to H_2S. c) Dynamic sensing response of **P1**, and **P2** devices to 4 ppm NO_2 gas at different time intervals. d) Sensitivity comparison of seven different gases at 4 ppm concentrations, where each error bar represents the sensitivity variation of four consecutive measurements at 4 ppm with the same device. All devices were operated at 500 mV.

200 s recovery period. The dynamic sensing responses of the devices toward different gases are presented in Figure 5a–c, and the calculated sensitivities of the sensors are detailed in Figure 5d and **Table** 2.

The **P1**-based device exhibited strong responses to 4 ppm NO_2, displaying a high average sensitivity of 588% ppm^{-1} as obtained from the measurement cycles (Figure 5c). Upon introducing 4 ppm SO_2, the device exhibited only slight increases in current, with an average sensitivity of +0.0365% ppm^{-1}. The marginal increase in current suggested the possibility of some electron transfer from the polymer to SO_2 molecules or occurrence of doping, although this effect was relatively weak. The device displayed a weak negative current response when exposed to NH_3, and an almost negligible current response to H_2S (Figure 5a). Since both polymers may have been lightly doped by atmospheric oxygen, electron-rich compounds such as ammonia and hydrogen sulfide might have caused a dedoping effect on the polymer, resulting in a decrease in current.[73,74] No response in current was observed for the **P1**-based device when 4 ppm CH_2O, C_2H_4, or H_2 was introduced.

The **P2**-based device exhibited very strong responses when 4 ppm NO_2 was introduced, achieving a high average sensitivity of +3010% ppm^{-1} (Figure 5c,d). Interestingly, this device exhibited only a very weak response to H_2S and no response to other five interfering gases (Figure 5b). The decrease in electric current signal when exposed to H_2S was associated with the previously

Table 2. Gas sensor sensitivity of **P1** and **P2** polymer toward seven different gases.

Gas	Polymer Chemiresistor Sensitivity (% ppm^{-1} ± std)[a]	
	P1 (130 °C annealed)	P2 (150 °C annealed)
Nitrogen dioxide (NO_2)	+588 (±31)	+3010 (±315)
Sulfur dioxide (SO_2)	+0.0365 (±0.0053)	0
Ammonia (NH_3)	−0.338 (±0.028)	0
Formaldehyde (CH_2O)	0	0
Ethylene (C_2H_4)	0	0
Hydrogen sulfide (H_2S)	−0.0823[b] (±0.0541)	−0.235[b] (±0.120)
Hydrogen (H_2)	0	0

[a] The standard deviation (std) value represents the sensitivity variation from four consecutive exposures to 4 ppm gas with the same device; [b] The negative response for this gas analyte is barely noticeable in both **P1** and **P2** based sensor devices. The responses were also relatively poor in terms of repeatability in dynamic sensing experiments.

mentioned dedoping process of the polymer. The sensitivity for 4 ppm H_2S was found to be −0.235% ppm^{-1}, which is considerably insignificant, being 1.28 × 10^4 times weaker when compared to the response to 4 ppm NO_2 gas. These findings highlight the remarkable selectivity of this sensor for NO_2. Figure S6 (Supporting Information) further illustrates the 4-ppm dynamic NO_2 sensing response of the **P2** polymer before and after the interfering gas experiments using the same 150 °C-annealed **P2** sensor device. These results provide strong evidence of the sensor's excellent reversibility.

To further demonstrate the practical applications of these sensors, we conducted dynamic NO_2 sensing response experiments using air as the carrier gas (Figure S7, Supporting Information). In addition, devices were also fabricated on flexible PET substrates, which are more compatible for the printing processes and wearable electronics applications. The **P2**-based device consistently exhibited superior response and recovery compared to the **P1**-based device. Notably, the PET-based device outperformed the SiO_2-based devices. These results strongly suggest that these polymers remain fully functional as NO_2 sensors in an air environment. Additionally, their ability to be deposited onto PET substrates holds promise for printable electronics applications.

In an effort to demonstrate the real-world utility of these sensors, we designed and constructed a proof-of-concept (POC) portable handheld NO_2 alarm system prototype using the all-solution-processed PET-based **P1** device. The device is powered by a standalone 9 V battery. We selected polymer **P1** for this purpose due to its higher baseline current and substantial absolute change in resistance response compared to **P2**. Figure S8 (Supporting Information) shows the set-up and general scheme of the electronic component of the NO_2 alert system. The simple circuit design did not require external amplifiers or transducers. Figure S8a (Supporting Information) demonstrates the activation of a blinking LCD screen and buzzer alarm system when the sensor is exposed to ≈0.1% NO_2 gas. A demonstration video simulating a ≈0.1% NO_2 gas leakage can be accessed in the Supporting Information. Figure S8c (Supporting Information) shows the schematic circuit diagram of the POC device. The potential applications of this technology range from personal safety devices for factory workers to large-scale gas leakage detection and emergency ventilation systems. Programming codes for the microcontroller can be found in the Supporting Information.

2.6. Study of Polymer-NO_2 Interaction through DFT Calculations

For an in-depth understanding of the electronic interaction between the polymers and NO_2 and to shed light on the sensing mechanism, we conducted density functional theory (DFT) calculations using the DMol3 code with generalized gradient approximation (GGA). To expedite the computational process, we employed a simplified model compound **I**, featuring methoxy substituents on the thiophene units and no side chains on the HID unit, thus representing the repeat units of **P1** and **P2** after the thermal removal of the carbamate chains (**Figure** 6a,b). Among various binding models explored between the model compound and NO_2 (Figure S9 and Table S1, Supporting Information), two predominant modes emerged, both involving DHB interactions between the amide moiety of HID and NO_2 (Figure 6a,b).

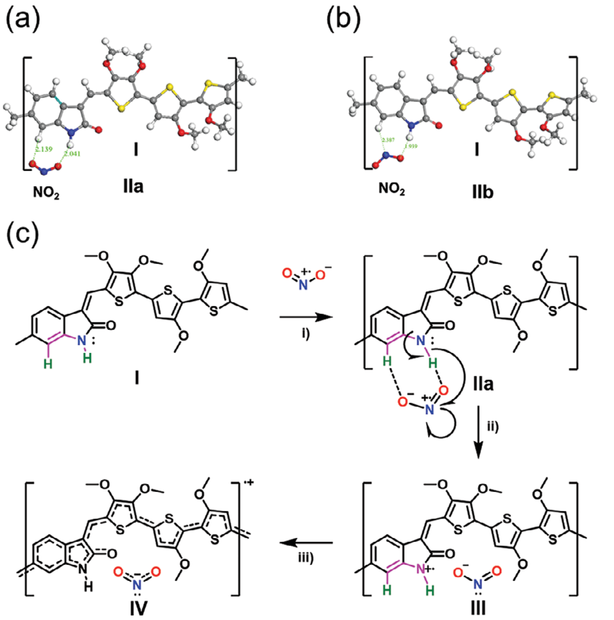

Figure 6. (a) and (b) present the two most stable binding modes (**IIa** and **IIb**) between NO_2 and a model molecule (**I**), representing **P1** and **P2**, respectively. In these modes, NO_2 and the unsubstituted amide group of HID establish dual hydrogen-bonds (DHB) with binding energies of 0.48 eV for mode (a) and 0.47 eV for mode (b). The DFT simulations involved optimizing molecular structures based on a geometric convergence criterion of energy at 1×10^{-5} eV and a residual force of 0.02 eV Å^{-1}. c) depicts the proposed electron transfer process (p-doping) from the model compound (**I**) to a NO_2 molecule: i) NO_2 accesses **I** by forming DHB, as shown in (a), leading to the formation of a complex **IIa**; ii) electron transfer from **I** to NO_2 in **IIa** results in the formation of a charge transfer complex **III**, generating a polaron (a radical cation) within **I**; iii) the polaron then delocalizes along the polymer main chain, ultimately achieving a p-doped state (**IV**).

In the first binding mode (a), DHB interactions occur between the two oxygen atoms of NO_2 and two hydrogen atoms from HID, forming complex **IIa**. One hydrogen atom comes from the amide —C(=O)NH— group, and the other is associated with the benzene ring, with bond lengths measuring 2.041 and 2.139 Å, respectively (Figure 6a). In this configuration, an electron transfer of 0.288 electrons from the polymer to NO_2 was observed, resulting in a binding energy of 0.48 eV. The second binding mode (b) also involves DHB, with one bond established between one oxygen atom of NO_2 and the amide hydrogen, and the other between the nitrogen atom of NO_2 and the HID benzene ring hydrogen atom, leading to the formation of complex **IIb**. The bond lengths in this arrangement measure 1.939 and 2.387 Å, respectively. In this case, the calculations indicated an electron transfer of 0.286 electrons from the polymer to NO_2, yielding a binding energy of 0.47 eV. It is noteworthy that the utilization of DHB has been documented as an effective strategy in the design of sensing materials with high selectivity, particularly in the context of NO_2 sensing.[39,75–78] Figure 6c illustrates the proposed electron transfer processes between the polymer and NO_2 via binding mode (a). In this process, NO_2 accesses the polymer model compound **I** through the formation of complex **IIa**, resulting in the

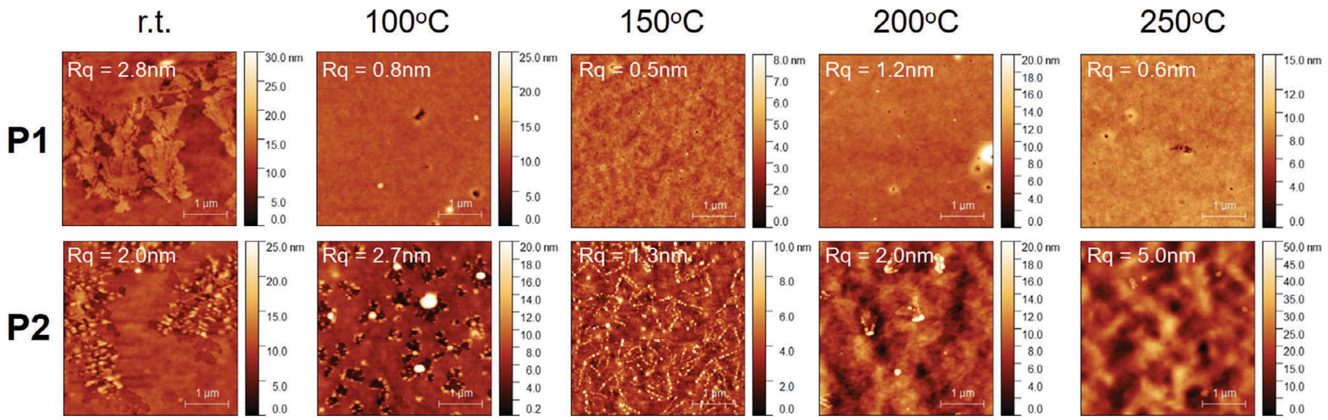

Figure 7. AFM height images of **P1** and **P2** thin films annealed at different temperatures (scale bar: 1 µm).

generation of a polaron (a radical cation) and ultimately leading to the p-doped state of the polymer (**IV**).

2.7. Investigation of the Sensitivity Dependence on Annealing Temperature

The sensitivity of **P1** and **P2**-based sensors displayed a strong dependence on the annealing temperature, as demonstrated in Figure 4. Generally, the sensitivity of a chemiresistive gas sensor is contingent upon several factors: 1) the strength of the interaction between analyte gas molecules and the sensing material, 2) the portion of the sensing material accessible to gas molecules, 3) the diffusion rate of analyte gas molecules into the active sensing material layer, and 4) the charge transport properties of the sensor material. All of these factors are intricately tied to the chemical composition and microstructure of the sensor material, which can be altered through thermal annealing.

One potential explanation for the sensitivity's dependence on annealing temperature lies in morphological changes within the film, which can influence the diffusion rate of NO_2 molecules. **Figure 7** presents atomic force microscopy (AFM) images of **P1** and **P2** films annealed at varying temperatures. The non-annealed (room temperature) **P1** film exhibits a root mean square roughness (Rq) of 2.8 nm. Up on annealing with temperatures ranging from 100 to 250 °C, the **P1** films become smoother, with decreased Rq values between 0.5 and 1.2 nm. However, no observable morphological alterations in the **P1** films could be correlated with the sensitivity's dependence on annealing temperature. For the **P2** films, the film roughness remains relatively consistent across annealing temperatures from room temperature to 200 °C. At an annealing temperature of 250 °C, the Rq of the film increases notably to 5 nm. This increase may be attributed to thermally induced chain movement, facilitated by the presence of long, flexible dodecyloxy side chains in this polymer. Similar to **P1**, **P2** also displays no clear sensitivity dependence on thermally induced morphological changes.

Additionally, the crystallinity or chain packing of the polymer gas-sensing material significantly impacts the sensor's sensitivity. Enhanced chain packing is favorable for charge carrier transport but can impede the diffusion of gas molecules.[79] X-ray diffraction (XRD) data reveals that the **P1** films remain amorphous at all annealing temperatures (Figure S10, Supporting Information). **P2** films exhibit amorphous characteristics when annealed below 150 °C. Films annealed at 200 and 250 °C exhibit weak (100) diffraction peaks, indicating the formation of short-ranged lamellar crystal structures. Nonetheless, the films remain highly disordered, implying that gas diffusion is unlikely to be substantially impeded. The XRD data thus suggests that the sensitivity's dependence on annealing temperature is not closely associated with changes in chain order within these polymer films.

The above results obtained from DFT simulations reveal that the unsubstituted amide —C(═O)NH— groups on the HID units have the ability to form robust DHB, thereby attracting NO_2 to the polymer backbone. It is worth noting that thermal decomposition of carbamate groups is likely initiated at temperatures ranging from ≈100 to 150 °C, liberating some —C(═O)NH— groups.[44,80] This may account for the notable increase in sensitivity observed in both **P1** and **P2** films at an annealing temperature of 150 °C. However, as the annealing temperature rises to 180 °C, and eventually 210 °C, both devices exhibit a diminishing sensitivity, ultimately losing their sensitivity entirely.

The TGA results indicate that at 150 °C for 20 min, 64% of carbamate chains are removed in **P1**, while 78% are removed at 250 °C for 20 min. For **P2**, 27% of carbamate chains are eliminated at 150 °C for 20 min, while 59% are removed at 250 °C for the same duration. These findings show that increasing the concentration of —C(═O)NH— groups does not always lead to an enhancement in NO_2 sensitivity.

A plausible hypothesis is that at a mild annealing temperature (e.g., 150 °C), carbamate side chains are partially removed, yielding a limited concentration of —C(═O)NH— groups. The steric effects arising from the side chains of the remaining carbamate groups and the lengthy dodecyloxy side chains keep the liberated —C(═O)NH— groups unbound, allowing them to interact individually with NO_2. Concurrently, the removal of carbamate side chains generates cavities between polymer chains, facilitating the access of NO_2 molecules to —C(═O)NH— groups (as illustrated in **Figure 8b**). These combined factors enhance the sensor's sensitivity.

However, at a higher annealing temperature (e.g., 250 °C), a significant number of carbamate groups are removed, yielding an excess of —C(═O)NH— groups (Figure 8c). The remaining side chains can no longer maintain separation between the main

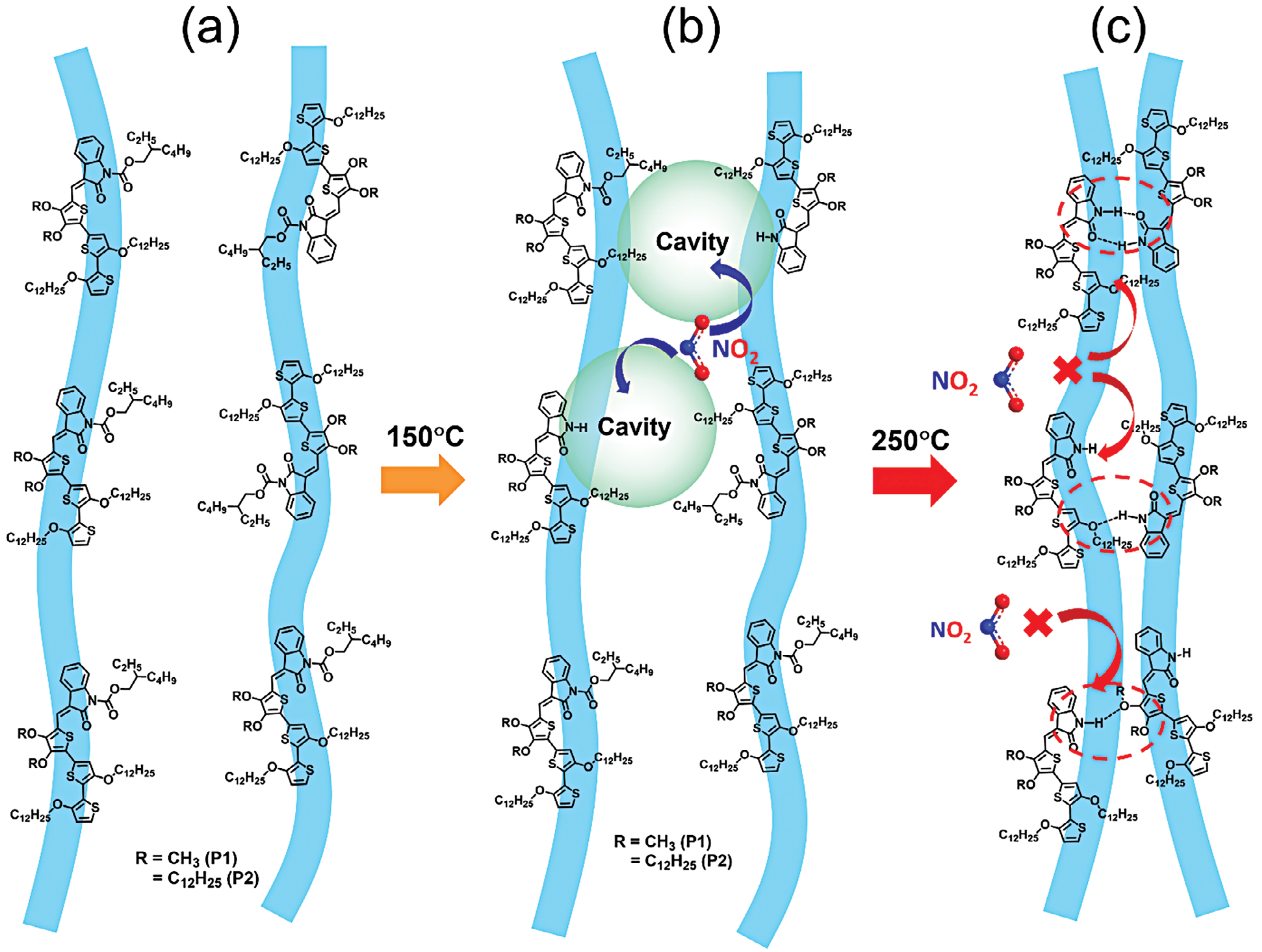

Figure 8. Schematic illustration of chains in the chemical structure of **P1** and **P2** caused by thermal annealing: a) Before thermal annealing; b) Annealed at mild temperatures (e.g., 150 °C), where some carbamate side chains are removed to create cavities and liberate a moderate amount of —C(═O)NH— groups that act as active sites to attract NO_2 molecules; c) Annealed at high annealing temperatures (e.g., 250 °C), where many carbamate side chains are removed to liberate an excessive amount of —C(═O)NH— groups, which form hydrogen bonds with —C(═O)NH— and alkoxy groups on the neighboring chains, hindering the entry of NO_2 molecules and weakening the —C(═O)NH— groups with NO_2 molecules.

polymer chains, causing the liberated —C(═O)NH— groups on one polymer chain to engage in tight hydrogen bonding with those on neighboring chains, a phenomenon observed in amide-containing polymers like Nylon-6 and Nylon-66.[46,81–83] Additionally, —C(═O)NH— groups can form hydrogen bonds with the ether C-O-C groups (methoxy and dodecyloxy in **P1** and **P2**) of adjacent polymer chains.[84–86] These hydrogen-bonded amide —C(═O)NH— groups tend to weaken or lose their capacity to interact with NO_2 molecules. Furthermore, the removal of excessive carbamate chains closes the cavities created by their absence, impeding NO_2 molecule diffusion. The formation of interchain hydrogen bonds introduces higher steric hindrance, further obstructing NO_2 molecules from accessing the polymer backbone and ultimately reducing the device's sensitivity. Notably, the ATR-IR spectra of samples **P1** and **P2** annealed at 250 °C exhibit a faint peak at 3444 cm^{-1}, corresponding to free N–H groups. This peak is superimposed on the broader peak representing hydrogen-bonded N-H groups (Figure 1), indicating the presence of a significant number of interchain hydrogen bonds.

3. Conclusion

This study introduced the design and synthesis of hemi-isoindigo (HID)-based polymers for highly sensitive and selective flexible NO_2 chemiresistive sensors. Two HID polymers, denoted as **P1** and **P2**, feature their thermally cleavable carbamate side chains, which create molecular cavities that enhance NO_2 diffusion upon thermal annealing. These polymers are further distinguished by their elevated HOMO energy levels of −4.74 and −4.77 eV, respectively. These elevated HOMO levels promote the formation of stable charge transfer complexes with the oxidizing gas NO_2, thereby enhancing NO_2 sensitivity.

Chemiresistive gas sensors were successfully developed utilizing **P1** and **P2** as active layers. Both **P1** and **P2**-based sensors exhibited p-type chemiresistive behavior, resulting in increased current upon exposure to NO_2 gas. When **P1** and **P2** films were subjected to annealing under optimized conditions, the sensors exhibited high sensitivities of +1400 and +3844%ppm^{-1}, low LOD values of 514 and 38.9 ppb, and remarkable selectivity for NO_2.

DFT calculations shed light on the mechanism of interaction between these polymers and NO_2. They reveal that the liberated amide moiety (—C(=O)NH—) and the adjacent hydrogen atom on the benzene ring of the polymer can readily engage with NO_2, forming dual hydrogen bonds (DHB) characterized by high binding energies. This interaction facilitates electron transfer from the polymer to NO_2. The unique interactions between the —C(=O)NH— groups and NO_2 also endow the **P1** and **P2**-based sensors with exceptionally high selectivity for NO_2 over other types of gases. Furthermore, it was observed that excessive formation of —C(=O)NH— groups at elevated annealing temperatures (>150 °C) leads to the development of interchain hydrogen bonds. This deactivates the —C(=O)NH— groups' ability to interact with NO_2 and hinders the diffusion of NO_2 into the polymer film. This work highlights the significant potential of HID-based polymers in high-performance NO_2 gas sensor applications. It also offers valuable insights into the structure-property relationships of conjugated polymers and the strategic design principles for developing high-performance gas sensors, paving the way for future advancements in this field.

Supporting Information

Supporting Information is available from the Wiley Online Library or from the author.

Acknowledgements

This work was supported by the Natural Sciences and Engineering Research Council of Canada (NSERC) through the Strategic Partnership Grants for Networks (SPGN) (NETGP 508526-17 and the Discovery Grants (RGPIN-2022-03835).

Conflict of Interest

The authors declare no conflict of interest.

Data Availability Statement

The data that support the findings of this study are available in the supplementary material of this article.

Keywords

conductive polymers, doped polymers, hemi-isoindigo, resistive sensors, temperature sensors

Received: November 2, 2023
Revised: January 15, 2024
Published online:

---

[1] M. Hodgson, H. Levin, P. Wolkoff, *J. Allergy Clin. Immunol.* **1994**, *94*, 296.
[2] J. W. Kwon, H. W. Park, W. J. Kim, M. G. Kim, S. J. Lee, *Environ. Health* **2018**, *17*, 65.
[3] E. Samoli, E. Aga, G. Touloumi, K. Nisiotis, B. Forsberg, A. Lefranc, J. Pekkanen, B. Wojtyniak, C. Schindler, E. Niclu, R. Brunstein, M. D. Fikfak, J. Schwartz, K. Katsouyanni, *Eur. Respir. J.* **2006**, *27*, 1129.
[4] A. Faustini, R. Rapp, F. Forastiere, *Eur. Respir. J.* **2014**, *44*, 744.
[5] WHO Working Group, Health Effects of Air Pollution with Particulate Matter, Ozone and Nitrogen Dioxide Dioxide, Bonn, Germany. Copenhagen : WHO Regional Office for Europe, **2003**, https://iris.who.int/handle/10665/107478.
[6] A. S. Lefohn, R. W. Brocksen, *J. Air Pollution Control Assoc.* **1984**, *34*, 1005.
[7] P. Grennfelt, A. Engleryd, M. Forsius, Ø. Hov, H. Rodhe, E. Cowling, *Ambio* **2020**, *49*, 849.
[8] D. A. Burns, J. Aherne, D. A. Gay, C. M. B. Lehmann, *Atmos. Environ.* **2016**, *146*, 1.
[9] P. M. Irving, *J. Environ. Qual.* **1983**, *12*, 442.
[10] J. L. Peel, R. Haeuber, V. Garcia, A. G. Russell, L. Neas, *Biogeochemistry* **2013**, *114*, 121.
[11] M. Guarnieri, J. R. Balmes, *Lancet* **2014**, *383*, 1581.
[12] I. Manisalidis, E. Stavropoulou, A. Stavropoulos, E. Bezirtzoglou, *Front. Public Health* **2020**, *8*.
[13] WHO/Europe, WHO guidelines for indoor air quality: selected pollutants, World Health Organization, **2010**, https://www.who.int/publications/i/item/9789289002134.
[14] G. Müller, A. Hackner, S. Beer, J. Göbel, *Materials* **2016**, *9*, 65.
[15] S. J. Choi, B. H. Jang, S. J. Lee, B. K. Min, A. Rothschild, I. D. Kim, *ACS Appl. Mater. Interfaces* **2014**, *6*, 2588.
[16] A. Dey, *Semiconductor Metal Oxide Gas Sens.* **2018**, *229*, 206.
[17] C. Wang, L. Yin, L. Zhang, D. Xiang, R. Gao, *Sensors* **2010**, *10*, 2088.
[18] A. Ponzoni, E. Comini, I. Concina, M. Ferroni, M. Falasconi, E. Gobbi, V. Sberveglieri, G. Sberveglieri, *Sens. Switz.* **2012**, *12*, 17023.
[19] K. K. Makhija, A. Ray, R. M. Patel, U. B. Trivedi, H. N. Kapse, *Bull. Mater. Sci.* **2005**, *28*, 9.
[20] E. Comini, G. Faglia, G. Sberveglieri, Z. Pan, Z. L. Wang, *Appl. Phys. Lett.* **2002**, *81*, 1869.
[21] Z. Liu, T. Yamazaki, Y. Shen, T. Kikuta, N. Nakatani, Y. Li, *Sens. Actuators, B* **2008**, *129*, 666.
[22] F. Zhang, Q. Lin, F. Han, Z. Wang, B. Tian, L. Zhao, T. Dong, Z. Jiang, *Microsyst. Nanoeng.* **2022**, *8*, 40.
[23] D. T. McQuade, A. E. Pullen, T. M. Swager, *Chem. Rev.* **2000**, *100*, 2537.
[24] J. Janata, M. Josowicz, *Nat. Mater.* **2003**, *2*, 19.
[25] M. W. Alam, S. Islam Bhat, H. S. Al Qahtani, M. Aamir, M. N. Amin, M. Farhan, S. Aldabal, M. S. Khan, I. Jeelani, A. Nawaz, B. Souayeh, *Polymers* **2022**, *14*, 2164.
[26] V. P. Elanjeitsenni, K. S. Vadivu, B. M. Prasanth, *Mater. Res. Express* **2022**, *9*, 022001.
[27] D. Liu, C. Huyan, Z. Wang, Z. Guo, X. Zhang, H. Torun, D. Mulvihill, B. B. Xu, F. Chen, *Mater. Horiz.* **2023**, *10*, 2800.
[28] H. Liu, Q. Li, S. Zhang, R. Yin, X. Liu, Y. He, K. Dai, C. Shan, J. Guo, C. Liu, C. Shen, X. Wang, N. Wang, Z. Wang, R. Wei, Z. Guo, *J. Mater. Chem. C* **2018**, *6*, 12121.
[29] H. Park, D. Kim, B. S. Ma, E. Shin, Y. Kim, T. Kim, F. S. Kim, I. Kim, B. J. Kim, *Adv. Sci.* **2022**, *9*, 2200270.
[30] I. Fratoddi, I. Venditti, C. Cametti, M. V. Russo, *Sens. Actuators, B* **2015**, *220*, 534.
[31] Z. Wang, L. Huang, X. Zhu, X. Zhou, L. Chi, *Adv. Mater.* **2017**, *29*, 1703192.
[32] S. Ji, H. Wang, T. Wang, D. Yan, *Adv. Mater.* **2013**, *25*, 1755.
[33] C. Liu, M. Wu, L. Gao, H. Liu, J. Yu, *Sens. Actuators, B* **2022**, *371*, 132540.
[34] G. G. Yang, D.-H. Kim, S. Samal, J. Choi, H. Roh, C. E. Cunin, H. M. Lee, S. O. Kim, M. Dincă, A. Gumyusenge, *ACS Sens.* **2023**, *8*, 3687.

[35] J. J. Miasik, A. Hooper, B. C. Tofield, *J. Chem. Soc. Faraday Trans. 1 Phys. Chem. Condens. Phases* **1986**, *82*, 1117.
[36] T. Hanawa, H. Yoneyama, *Synth. Met.* **1989**, *30*, 341.
[37] L. Gao, C. Liu, Y. Peng, J. Deng, S. Hou, Y. Cheng, W. Huang, J. Yu, *Sens. Actuators, B* **2022**, *368*, 132113.
[38] M. Procek, K. Kepska, A. Stolarczyk, *Sensors* **2018**, *18*, 928.
[39] J. Zhou, H. Lin, X. F. Cheng, J. Shu, J. H. He, H. Li, Q. F. Xu, N. J. Li, D. Y. Chen, J. M. Lu, *Mater. Horiz.* **2019**, *6*, 554.
[40] E. Zampetti, S. Pantalei, S. Scalese, A. Bearzotti, F. De Cesare, C. Spinella, A. Macagnano, *Biosens. Bioelectron.* **2011**, *26*, 2460.
[41] H. Tai, Y. Jiang, G. Xie, J. Yu, X. Chen, *Sens. Actuators, B* **2007**, *125*, 644.
[42] J. Lu, D. Liu, J. Zhou, Y. Chu, Y. Chen, X. Wu, J. Huang, *Adv. Funct. Mater.* **2017**, *27*, 1700018.
[43] J. Liang, Z. Song, S. Wang, X. Zhao, Y. Tong, H. Ren, S. Guo, Q. Tang, Y. Liu, *ACS Appl. Mater. Interfaces* **2020**, *12*, 52992.
[44] J. H. L. Ngai, J. Polena, D. Afzal, X. Gao, M. Kapadia, Y. Li, *Adv. Funct. Mater.* **2022**, *32*, 2110995.
[45] J. H. L. Ngai, X. Gao, P. Kumar, J. Polena, Y. Li, *Adv. Electron. Mater.* **2021**, *7*, 2000935.
[46] L. R. Schroeder, S. L. Cooper, *J. Appl. Phys.* **1976**, *47*, 4310.
[47] D. J. Skrovanek, S. E. Howe, P. C. Painter, M. M. Coleman, *Macromolecules* **1985**, *18*, 1676.
[48] R. Puffr, J. Šebenda, *J. Polym. Sci. Part C Polym. Symp.* **1967**, *16*, 79.
[49] L. Han, K. Zhang, H. Ishida, P. Froimowicz, *Macromol. Chem. Phys.* **2017**, *218*, 1600562.
[50] K. S. Maiti, A. Samsonyuk, C. Scheurer, T. Steinel, *Phys. Chem. Chem. Phys.* **2012**, *14*, 16294.
[51] P.-H. Huang, C.-H. Tseng, C.-Y. Lin, C.-W. Lee, F.-L. Yen, *Int. J. Nanomed.* **2018**, *13*, 3279.
[52] B. S. Ong, Y. Wu, P. Liu, S. Gardner, *J. Am. Chem. Soc.* **2004**, *126*, 3378.
[53] D. R. Miller, S. A. Akbar, P. A. Morris, *Sens. Actuators, B* **2014**, *204*, 250.
[54] J. Pommerehne, H. Vestweber, W. Guss, R. F. Mahrt, H. Bässler, M. Porsch, J. Daub, *Adv. Mater.* **1995**, *7*, 551.
[55] T. Mukhopadhyaya, J. S. Wagner, H. Fan, H. E. Katz, *ACS Appl. Mater. Interfaces* **2020**, *12*, 21974.
[56] H. Li, J. Dailey, T. Kale, K. Besar, K. Koehler, H. E. Katz, *ACS Appl. Mater. Interfaces* **2017**, *9*, 20501.
[57] B. Shao, Y. Liu, X. Zhuang, S. Hou, S. Han, X. Yu, J. Yu, *J. Mater. Chem. C* **2019**, *7*, 10196.
[58] J. Choi, B. H. R. Suryanto, D. Wang, H.-L. Du, R. Y. Hodgetts, F. M. Ferrero Vallana, D. R. MacFarlane, A. N. Simonov, *Nat. Commun.* **2020**, *11*, 5546.
[59] S. Trasatti, *Pure Appl. Chem.* **1986**, *58*, 955.
[60] M. S. A. Abdou, F. P. Orfino, Z. W. Xie, M. J. Deen, S. Holdcroft, *Adv. Mater.* **1994**, *6*, 838.
[61] M. S. A. Abdou, F. P. Orfino, Y. Son, S. Holdcroft, *J. Am. Chem. Soc.* **1997**, *119*, 4518.
[62] S. Hoshino, M. Yoshida, S. Uemura, T. Kodzasa, N. Takada, T. Kamata, K. Yase, *J. Appl. Phys.* **2004**, *95*, 5088.
[63] H.-H. Liao, C.-M. Yang, C.-C. Liu, S.-F. Horng, H.-F. Meng, J.-T. Shy, *J. Appl. Phys.* **2008**, *103*, 104506.
[64] S. Gambino, *Thin Solid Films* **2021**, *718*, 138485.
[65] F. Allegrini, A. C. Olivieri, *Anal. Chem.* **2014**, *86*, 7858.
[66] A. Shrivastava, V. Gupta, *Chron. Young Sci.* **2011**, *2*, 21.
[67] Ed.: V. Gold, *The IUPAC Compendium of Chemical Terminology: The Gold Book*, 4th ed., International Union of Pure and Applied Chemistry (IUPAC), Research Triangle Park, NC **2019**
[68] J. Z. Ou, W. Ge, B. Carey, T. Daeneke, A. Rotbart, W. Shan, Y. Wang, Z. Fu, A. F. Chrimes, W. Wlodarski, S. P. Russo, Y. X. Li, K. Kalantar-zadeh, *ACS Nano* **2015**, *9*, 10313.
[69] Y. Zhang, J. J. Kim, D. Chen, H. L. Tuller, G. C. Rutledge, *Adv. Funct. Mater.* **2014**, *24*, 4005.
[70] J.-H. Yoon, J.-S. Kim, *Solid State Ion.* **2011**, *192*, 668.
[71] R. Kumar, X. Liu, J. Zhang, M. Kumar, *Nano-Micro Lett.* **2020**, *12*, 164.
[72] T. Pham, G. Li, E. Bekyarova, M. E. Itkis, A. Mulchandani, *ACS Nano* **2019**, *13*, 3196.
[73] T. P. A. van der Pol, S. T. Keene, B. W. H. Saes, S. C. J. Meskers, A. Salleo, Y. van de Burgt, R. A. J. Janssen, *J. Phys. Chem. C* **2019**, *123*, 24328.
[74] I. E. Jacobs, F. Wang, N. Hafezi, C. Medina-Plaza, T. F. Harrelson, J. Li, M. P. Augustine, M. Mascal, A. J. Moulé, *Chem. Mater.* **2017**, *29*, 832.
[75] Y. Wang, D. Liu, J. Yin, Y. Shang, J. Du, Z. Kang, R. Wang, Y. Chen, D. Sun, J. Jiang, *Chem. Commun.* **2020**, *56*, 703.
[76] A. Kumar, R. Meunier-Prest, M. Bouvet, *Sensors* **2020**, *20*, 4700.
[77] X. Wang, H. Wang, X. Ding, X. Wang, X. Li, Y. Chen, *Org. Electron.* **2017**, *50*, 389.
[78] L. Guo, Y. W. Hao, P. L. Li, J. F. Song, R. Z. Yang, X. Y. Fu, S. Y. Xie, J. Zhao, Y. L. Zhang, *Sci. Rep.* **2018**, *8*.
[79] K. Potje-Kamloth, *Crit. Rev. Anal. Chem.* **2002**, *32*, 121.
[80] C. Guo, J. Quinn, B. Sun, Y. Li, *J. Mater. Chem. C* **2015**, *3*, 5226.
[81] D. Garcia, H. W. Starkweather, *J. Polym. Sci. Polym. Phys. Ed.* **1985**, *23*, 537.
[82] N. S. Murthy, *J. Polym. Sci. Part B Polym. Phys.* **2006**, *44*, 1763.
[83] A. I. Alateyah, Y. El-Taybany, S. El-Sanabary, W. H. El-Garaihy, H. Kouta, *Polymers* **2022**, *14*, 3585.
[84] I. S. Ryu, X. Liu, Y. Jin, J. Sun, Y. J. Lee, *RSC Adv.* **2018**, *8*, 23481.
[85] T. Zheltonozhskaya, N. Permyakova, L. Momot, in *Hydrogen-Bonded Interpolymer Complexes*, World Scientific, Singapore **2009**, pp. 85–154.
[86] V. V. Khutoryanskiy, G. Staikos, *Hydrogen-Bonded Interpolymer Complexes: Formation, Structure and Applications*, World Scientific, Singapore **2009**